Solid-state chemistry of inorganic fluorides: From tungsten-bronze types to functionalized nanofluorides: A review

Alain Tressaud

Journal of Fluorine Chemistry 281 (2025) 110374

Contents lists available at ScienceDirect

Journal of Fluorine Chemistry

journal homepage: www.elsevier.com/locate/fluor

Solid-state chemistry of inorganic fluorides: From tungsten-bronze types to functionalized nanofluorides: A review

Alain Tressaud

ICMCB-CNRS, University Bordeaux, 33600 Pessac, France & European Academy of Sciences, 11 Rue d'Egmont, Brussels, Belgium

ARTICLE INFO

Keywords:
Solid-state chemistry of inorganic fluorides
Bronze-type fluorocomponds
Hexagonal tungsten bronze (HTB)
Tetragonal tungsten bronzes (TTB)
Defect pyrochlore
UV absorbers, Multiferroic component
Catalytic activity
Structural phase transition

ABSTRACT

Solid-state chemistry of inorganic fluorides has gained great importance in the second half of 20th century. It aims at identifying the relationships between the structural networks and the physical properties resulting from interactions within these networks. One of the most significant results was the discovery in the 1960s of series of A_xMF_3 fluorides with structures similar to those of tungsten oxide bronzes. The investigation of other compounds mainly based on Al, Ga and transition metals with structures derived from ReO_3, hexagonal tungsten bronze (HTB), tetragonal tungsten bronzes (TTB), defect pyrochlore and perovskite was soon launched in relation, in a first step, to their magnetic properties. Such interest was further extended to various properties such as positive electrodes in Li-ion batteries, UV absorbers, multiferroic components. Today, solid-state inorganic fluorides are present at the nano-sized level as components in many advanced technologies, including Li batteries or all solid-state fluorine batteries, micro- or nano-photonics, up- or down-conversion fluorescent probes, solid-state lasers, nonlinear optics, nuclear cycle, superhydrophobic coatings, etc. It has been pointed out that most of these outstanding properties can be correlated to the exceptional electronic properties of elemental fluorine, F_2.

The aim of this article is to review the solid-state chemistry of fluorides having the formula A_xMF_3 over several decades, from their discovery in the 1960s to the interesting physical-chemical properties more recently investigated on these phases that derive from the ReO_3, perovskite, defect-pyrochlore, hexagonal- and tetragonal-tungsten bronze types.

1. Introduction

In the second part of the 20th century, a new research direction emerged: "Solid-state Chemistry". The goals consisted of identifying the relationships existing between ionocovalent structural networks and exceptional physical properties that resulted from interactions within these networks. These types of considerations arose largely from the innovative studies which had allowed Linus Pauling to derive the famous "Pauling's rules" for atomic arrangements in crystals with ionic bonding, such as the radius-ratio rule and coordination polyhedra, electrostatic valency, different types of connections between polyhedra, i.e., through corners, edges or faces, sharing of different cations, with large valence and small coordination number [1].

Due to the much more ionic character of metal-fluorine bonds, transition-metal fluorides were indeed excellent examples for verifying "Pauling's rules". The importance of radius-ratio rules on the final networks can be illustrated by the impact of the Goldschmidt tolerance factor t, in $A^{+}B^{2+}F_3$ perovskites (Fig. 1). The compacity factors are illustrated for $t > 1$ and $t < 1$. (Note that $GdFeO_3$-type fluoroperovskites serve today as models of post-post-perovskites at high pressure conditions and have an impact on the mineralogy and rheology of the deep region at the base of the Earth's mantle. There is no need to point out the importance of perovskite compounds in many fields, in particular as perovskite halide [formamidinium (FA) lead iodide, $FAPbI_3$] in perovskite solar cells (PSC), and the hexagonal fluoro-perovskites are relevant models for quantum materials because several hexagonal oxide perovskites are candidates for illustrating the quantum-spin-liquid state at low-temperature [2]).

Among several important events in the rise of the discipline is the "International Conference on Transition Metal Oxides" in Bordeaux (October 1964), a symposium in which big names in chemistry, physics and the materials sciences participated. Among these specialists was John B. Goodenough who developed the approach of a solid-state chemist that involved the crystal-field description of the ionic solids, the molecular description of the chemical bond, and the physicist's view of the delocalized outer-electrons, as he had just conceptualized in his book "Magnetism and the Chemical Bond" [3].

At the same time, a French scientist from Bordeaux, Robert de Pape,

E-mail address: atressaud@gmail.com.

https://doi.org/10.1016/j.jfluchem.2024.110374
Received 30 August 2024; Received in revised form 28 November 2024; Accepted 29 November 2024
Available online 6 December 2024

published a decisive paper on "*A series of bronze-type fluorinated compounds*" [4] having the formulation K_xFeF_3 (with $0 \leq x \leq 1$). The system contained several original phases similar to those of the tungsten bronzes K_xWO_3 which were so named by A. Magnéli because of their color [5]. In this iron fluoride series, a large variety of structure types were observed depending on the x-value, which were all characterized by (FeF_6) octahedra connected at corners (Fig. 2). A variety of different structure types were obtained depending on the value of x and size of the alkali metal. Because of possible varied intercalation rates of the monovalent cations within the structure, these phases exhibited several stability ranges, as shown in Table 1. The charge balance is compensated by a change in the oxidation state of the transition element. Soon after the discovery of K_xFeF_3 tungsten bronze-type fluoro-compounds, investigations of similar compounds were launched with a particular interest in the relationships between structural types and magnetic properties [6–11].

These series were later generalized by the discovery of numerous $A_x(M^{II}_xM^{III}_{1-x})F_3$ structural types with mixed oxidation states and containing differently connected (MF_6) octahedra where M = Al, Ga, d-transition element. Metal fluoride compounds with the general formula A_xMF_3 adopt several networks including the ReO_3 (rhombohedral, Space Group: R-3c), the pyrochlore (cubic, S.G.: $Fd\bar{3}m$, the Tetragonal Tungsten-Bronze, denoted as TTB (tetragonal, S.G.: P4/mbm) or the Hexagonal-Tungsten-Bronze (denoted as HTB, orthorhombic, S.G: Cmcm) types [12–14].

The present review takes into account the initial work that began in the 1960s until the very recent results obtained on these types of compounds and similar phases. Several examples of fluorinated compounds exhibiting structural networks have been selected such as, ReO_3, perovskite, defect pyrochlore, hexagonal and tetragonal tungsten bronzes, in order to point out the great diversity of physical-chemical properties among these phases.

2. Experimental: the microwave-assisted fluoro-hydrothermal route

Besides the conventional methods of solid-state chemistry, i.e., firing at high temperature of the starting components, gaseous or plasma fluorination, conventional fluoro-hydrothermal methods, decomposition processes, the microwave-assisted technique has been used to prepare aluminum and transition element fluoro-compounds. at low temperatures. This technique, which was launched in Bordeaux by A. Demourgues, D. Dambournet and N. Penin, has been shown to be suitable for the achievement of high-surface-area metal-based fluorides [15–17].

The microwave-assisted procedure for aluminum hydroxy-fluorides is given here as an example. These phases have aroused considerable interest because of their high catalytic activity in halogen-exchange reactions, and because they are able to favor the conversion of ozone-depleting CFCs to more environmentally acceptable HFCs [18–20].

Among the three different forms that can be prepared, β-$AlF_{2.5}(OH)_{0.5}$, with the HTB structure [21], is obtained from the aluminum nitrate precursor according to the following procedure: a solution containing the aluminum precursor, water, with isopropanol as solvent was mixed in an aqueous solution of HF (40%) in the molar ratio, [HF]/[Al] = 3.0. After the microwave hydrothermal process, the resulting powder was washed with a large amount of ethanol under nitrogen, and then outgassed at 300°C under vacuum for 4 h. Elemental analysis, FTIR and NMR spectroscopies allowed control of the final chemical composition, showing the presence of both NH_4^+ and H_2O as residual species inside the network. This result can be related to the reduction of nitrate ions to ammonium ions during the microwave hydrothermal process, which permits the stabilization of the HTB network thanks to a template effect. Due to the occurrence of water and ammonium ion that are trapped to the network, the thermal stability of the resulting compound is similar to that of the compound prepared in the conventional way using thermal treatment of β-$AlF_3{\cdot}3H_2O$ (with HTB structure) or $(NH_4)_3AlF_6$. However, the different hydroxyl contents induce different thermal behavior and physical-chemical properties.

3. Nanosized M(OH, F)$_3$ metal hydroxyfluorides: correlations among structural features, thermal stability and acidic properties

Although inorganic oxides are active acidic heterogeneous catalysts in organic reactions such as alkylation and acylation of aromatic compounds, polymerization and halogen exchange, the incorporation of a more electronegative species such as fluoride anion allows the catalyst activity to increase by enhancing its acidic properties. Under these conditions, the number and strength of Brønsted/Lewis acid sites and the specific areas of the materials appear to be the key factors that determine their activities [18–20,22].

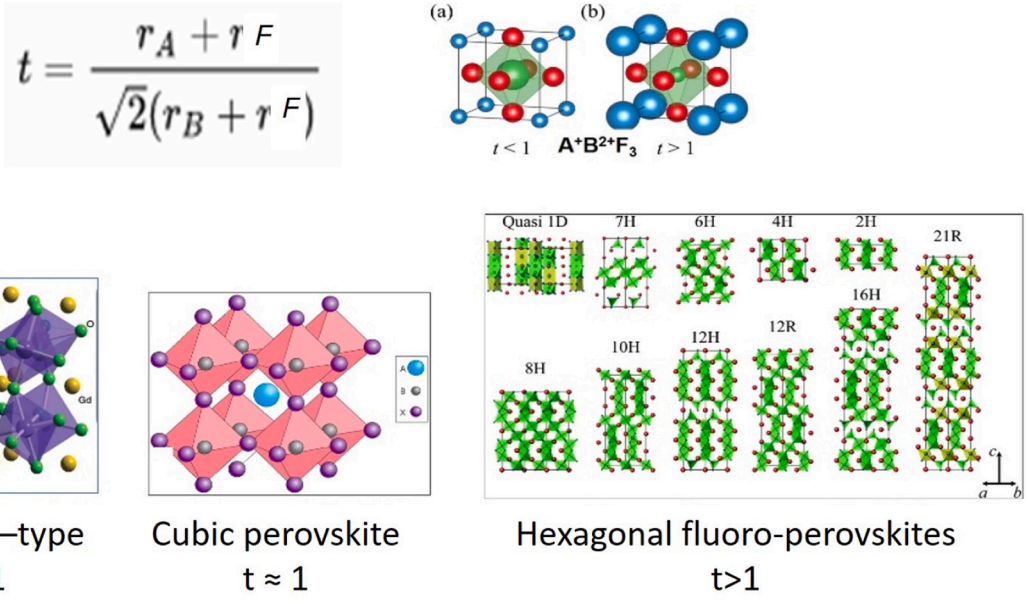

Fig. 1. Importance of the Goldschmidt tolerance factor, t, on the structural networks of $A^+B^{2+}F_3$ fluoroperovskites.

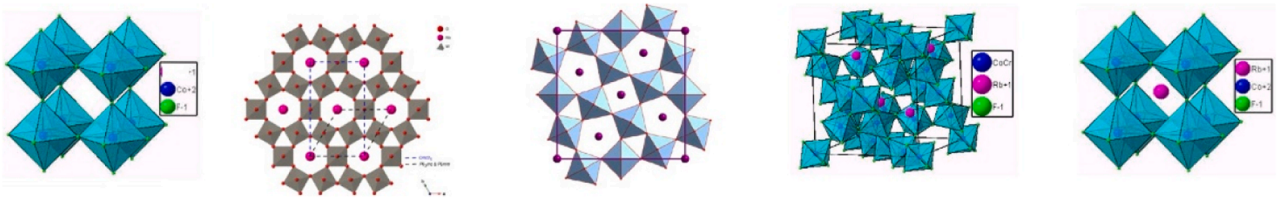

Fig. 2. Different structural networks observed in A_xFeF_3 (with $0 \leq x \leq 1$). [From the left to right: ReO_3, Hexagonal tungsten bronze (HTB), Tetragonal tungsten bronzes (TTB), Defect pyrochlore, Perovskite].

Table 1
Stability domains of $A_x(Fe^{II}_xFe^{III}_{1-X})F_3$ compounds ($0 \leq x \leq 1$).

A	HTB	TTB	Pyrochlore
K	$0.18 < x < 0.25$	$0.40 < x < 0.60$	
Rb	$0.18 < x < 0.30$		$0.43 < x < 0.58$
Cs	$0.19 < x < 0.27$		$0.48 < x < 0.53$
Tl	$0.20 < x < 0.31$		$0.49 < x < 0.56$
NH_4	$0.18 < x < 0.31$		$0.48 < x < 0.56$

Table 2
Dependence of the final surface area of the pyrochlore Al hydroxyfluoride on the type of precursor and solvents (HF/Al molar ratio ≈ 2; solvothermal reaction at 160°C, 1 h).

Al^{3+} precursor	Types of solvents and volume ratio	Surface area ($m^2\ g^{-1}$)
Nitrate	Isopropanol/water: 1/1	6
Isopropoxyde	Isopropanol/water: 1/1	77
Isopropoxyde	Isopropanol/water/ether: 1/1/0.3	137

Depending on various experimental conditions: temperature, pressure conditions and above all, the choice of the metal precursor and the [HF]/[M] ratio, ReO_3- HTB-, and pyrochlore-types can be alternatively synthesized depending on the Al precursor and the F/Al molar ratio, as shown in Fig. 3.

The drastic influence of microwave-assisted fluoro-hydrothermal conditions on the final surface area is given in Table 2 for the pyrochlore form, and the sizes of nano-particles of the different forms of aluminum hydroxyfluorides are compared in Fig. 4 [23,24]. Note that, analogous to the microwave assisted technique, the conventional mild-hydrothermal methods also yields different kinetically stabilized fluorides, including HTB and pyrochlore, by adjusting the reaction conditions. The structural parameters and compositions of high-surface-area (HSA) Al hydroxy-fluorides, are given in Table 3.

The acidic properties have been demonstrated by FTIR analysis and adsorption of pyridine and CO probe molecules. For example, at 300°C both strong Lewis and Brønsted acidities have been observed in the ReO_3 form of Al hydroxyfluoride together with an equivalent number of sites revealing bifunctionality. The strongly acidic behavior highlights the effect of water molecules and cationic vacancies on the surface structure. Whereas the Lewis acid strength progressively decreases with dehydration, the Brønsted acidity remains strong, even at 500°C. The strongest Lewis acidity, as found in homologous Al^{3+} and Ga^{3+} compounds, can be directly related to the strengths of the M–(F,OH) chemical bonds and to the thermal stabilities of these solids. The ratio χ/r^2 (χ, electronegativity and r, ionic radius), can be assigned to an electrical field gradient around the cation, and can explain some important acidic trends in the series. This parameter has allowed a more accurate approach to both the acid strength and the thermal stability and has accounted for the experimentally observed sequence [17–19].

The Cr^{3+}, Fe^{3+}, Ga^{3+}-based HTB phases of general formula β-$MF_{3-x}(OH)_x$. zH_2O, with M = Cr, Fe, Ga, were prepared either by sol precipitation followed by thermal treatments or by microwave-assisted techniques. The thermal stabilities of these compounds depend on the

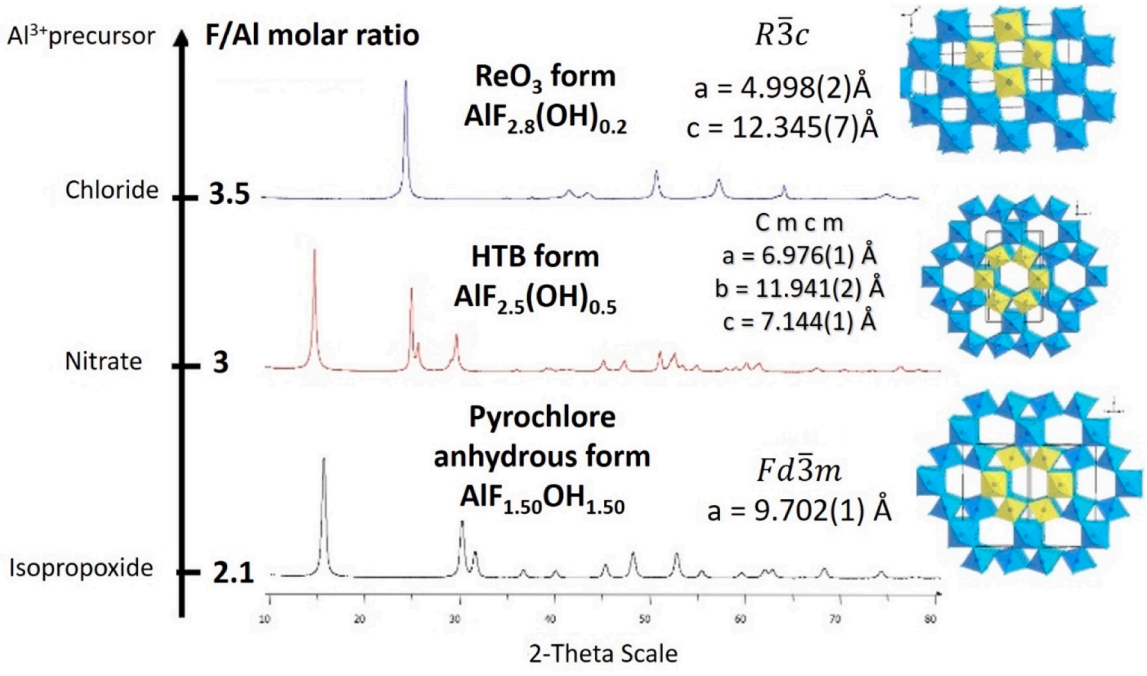

Fig. 3. Dependence of Al hydroxyfluoride structural networks and X-ray diffractograms (XRD) on the microwave experimental parameters.

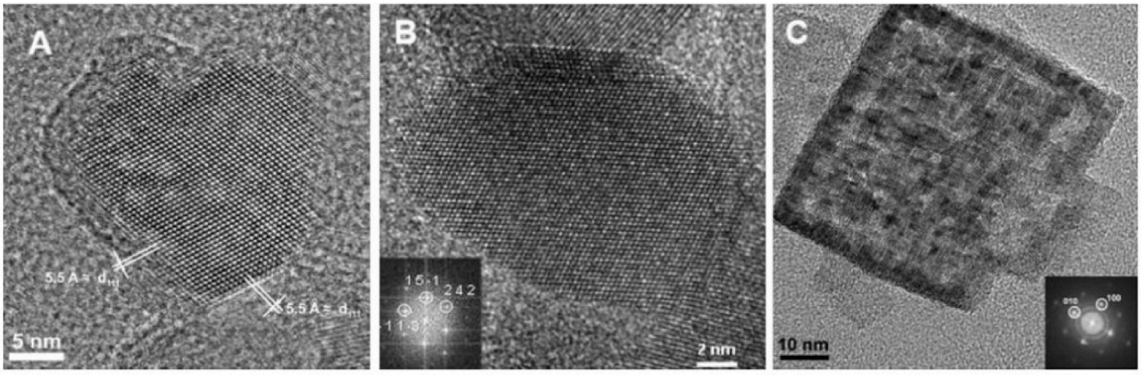

Fig. 4. High-resolution transmission electron micrographs (HRTEM) of nano-particles of Al-based hydroxyfluoride materials: (A) pyrochlore-, (B) HTB- and C) ReO_3-derived forms [from refs. 23,24].

Table 3
Compositions and structural characteristics of HSA Al hydroxy-fluorides.

Structure type	Composition	Symmetry	Unit cell (Å)	Distances and angles
ReO_3-derived	$Al_{0.82}\square_{0.18}F_{2.46}(H_2O)_{0.54}$	Cubic, $Pm\bar{3}m$, Z = 1	a = 3.6067(1)	Al–F: 1.8034(1) Å F–F: 2.5503(1) Å
HTB-derived	$AlF_{2.6}(OH)_{0.4}$	Orthorhombic, Cmcm, Z = 12	a = 6.9681(2) b =12.0360(3) c = 7.1434(1)	1.77(3) < Al–(F,O) < 1.86(1) Å 140 < Al–(F,O)–Al <173 °
Pyrochlore	$AlF_{1.8}(OH)_{1.2}.\varepsilon H_2O$	Cubic, $Fd\bar{3}m$, Z = 1	a = 9.7309(1)	Al–(O,F): 1.824(1) Å Al–F–Al: 141.12(6)°

natures of the cations, the decomposition kinetics of the $M(H_2O)_6^{3+}$ aquo-complexes and the sizes of the tunnels in the HTB framework. For instance, in Al^{3+} and Fe^{3+} hydroxyfluorides, the Al–(F,OH) bond is more stable than the Fe–(F,OH) bond, with a difference of more than 200 K in their thermal stabilities. The substitution of Fe^{3+} by Cr^{3+}, leads to an increase in the content of H_2O/OH groups preferentially around Cr^{3+}, allowing improvement of the M–F bond stability. The acidic characters of these compounds has been characterized by FTIR analysis using probe molecule adsorption. The results have shown that Al^{3+} and Ga^{3+} compounds exhibit stronger Lewis acidity than the homologous iron hydroxyfluorides. This information can be directly correlated to the strength of the M–(F,OH) chemical bonds and the thermal stabilities of these solids [24].

4. Electrochemical performance in Li batteries of iron hydroxyfluorides with the Hexagonal Tungsten Bronze (HTB) structure

An iron-based hydroxyfluoride with a Hexagonal Tungsten Bronze (HTB) network can be stabilized using microwave-assisted synthesis. The determination of the chemical composition yields $FeF_{2.2}(OH)_{0.8}.(H_2O)_{0.33}$. The HTB-type structure is stable from room temperature to 350°C under an Ar flow without any fluorine loss and only water loss. Between 200°C and 350°C, the chemical composition can be modified depending on the different amounts of OH^-/O^{2-} and structural water. By an adapted thermal treatment of dehydroxylation, anionic vacancies can be stabilized within the HTB network to yield a composition corresponding to $FeF_{2.2}(OH)_{0.8-x}O_{x/2}\square_{x/2}$. XRD Rietveld analysis, the atomic pair distribution function (PDF) and Mössbauer spectroscopy confirm the presence of iron atoms in an under-coordinated octahedral environment: $FeX_5\square_1$ (X = O^{2-}, F^-, OH^-) [25]. During the redox process, the distribution of various anions (O^{2-}, F^-, OH^-) and vacancies around Fe can be tuned by suitable polarization of the Fe–X chemical bonding. Fe-based oxyfluoride containing a higher proportion of O^{2-} and anionic vacancies as well as the lower content of structural water and hydroxyl groups best exhibit electrochemical performance. Charge and discharge curves for Li/ "Fe(F,OH)" cells in a non-aqueous electrolyte are given in Fig. 5 at a current density of 50 mA/g. The positive active material is HTB-type $FeF_{2.2}(OH)_{0.8}.(H_2O)_{0.33}$ annealed at 350°C under an Ar flow [25].

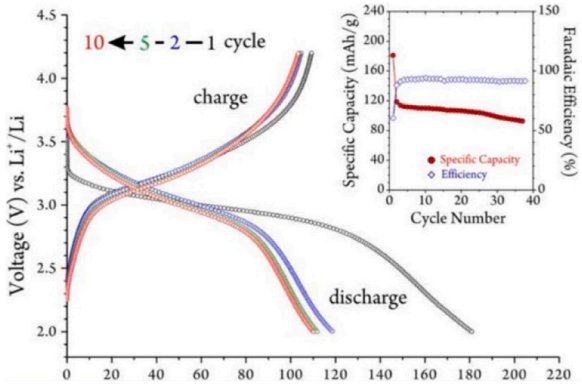

Fig. 5. Cyclic voltammetry charge and discharge curves for Li/ "Fe(F,OH)" cells in a non-aqueous electrolyte [from ref. 25].

Reviews on the use of fluorinated materials as positive electrodes for Li- and Na-ion batteries have recently appeared [26] and Fe-based fluorinated electrode materials have been discussed in terms of four classes of materials: metal fluorides, fluorine-based polyanionic compounds, carbon fluorides, and fluorine-substituted/surface-fluorinated electrode materials [27].

5. UV shielding properties and dual electrochemical properties in titanium hydroxyfluoride derived from the ReO_3 structure

It has been noted that microwave syntheses allow the preparation of metastable phases with unusual chemical behaviors that are illustrated by the acidic properties of Al-based compounds, and the UV shielding properties of ReO_3-derived Ti^{4+} hydroxyfluoride. Using lower molar ratios, R = F/Ti, two other Ti-based networks, i.e., hexagonal tungsten

bronze and anatase types can be synthesized as shown in Fig. 6 for Ti^{4+}, and pyrochlore, HTB- and ReO_3-types for Fe^{3+} systems [28–30].

A new Ti hydroxyfluoride, which crystallized in a ReO_3-derived network, was obtained using the microwave-assisted route. A superstructure for the ReO_3 network was proposed with two Ti sites and two anionic (OH/F) positions. Titanium vacancies are present in the structure and hydroxyl groups and are in the vicinity of the Ti^{4+} cations. All physical characterizations yielded the chemical formula $Ti_{0.75}\square_{0.25}(OH)_{1.5}F_{1.5}$. Refinements of the powder XRD and neutron diffractograms confirm the $Pn\bar{3}m$ space group with isotropic $TiX_{6/2}$ octahedra and elongated $TiY_{4/2}X_{2/2}$ (X, Y = OH, F) octahedra, where Ti vacancies are mainly located in the latter distorted site as determined by valence bond calculations, whereas F^-/OH^- are randomly distributed over the two anionic sites, as shown in Fig. 7.

Titanium hydroxyfluoride, $Ti_{0.75}(OH)_{1.5}F_{1.5}$, has been proposed as a UV absorber with an absorption edge around 3.2 eV -as the TiO_2 anatase form- but with a lower refractive index (n = 1.9 in the visible range [28]. The O(2p)-Ti(3d) charge transfer band, which is responsible for this absorption, implies OH groups and the nonbonding character of the 2p valence band. The low value of the optical band gap, despite the short Ti–O/F bond distance, can be explained by the stabilization of OH groups in the vicinity of Ti^{4+} cations. This results in the destabilization of the 2p (O) valence band with nonbonding character because of the presence of protons and Ti vacancies [28–31].

In the field of Li batteries, electrodes based on multielectron redox processes can overcome the limitation due to intercalation chemistry, in which only up to a single electron is transferred per redox-active metal ion. The materials undergo reversible reduction to form metal nanoparticles M^0 and binary Li compounds, following the reaction: $M^{z+}X_Y + zLi^+ + ze^- \leftrightarrow M^0 + yLi_{z/y}X$ [32]. Mixed-anion oxy- or hydroxyfluorides offer an attractive compromise, because of their reduced polarization, tunable redox potentials, and improved cycle stability [33]. Nanoscale (~80 nm) vacancy-containing titanium hydroxyfluoride, derived from the ReO_3-type, is not the electroactive component responsible for the reversible energy storage unlike other mixed anion systems [34]. Instead, the initial discharge (lithiation) process induces an irreversible dissociation of the hydroxyfluoride into oxide- and fluoride-rich phases. These components are involved in two reversible processes: intercalation and conversion processes, respectively [35].

6. Thermodynamic properties and structural phase transitions in iron fluorides with the Tetragonal Tungsten Bronze (TTB) type

Transition metal fluorides with the general formulation $K_{6-x}M^{2+}_{6-x}M^{3+}_{4+x}F_{30}$ (M = transition metal), similar to the general formula $K_{0.5}MF_3$, adopt the tetragonal tungsten bronze (TTB) structure. These phases may be of interest as potential multiferroic materials. It has been shown that members of this series may be multiferroic at low temperatures. The relationships between ferroelectricity, ferroelasticity and magnetic ordering parameters can be precisely adjusted by modifying the compositions. The presence of both ferroelectric and ferroelastic behavior had been shown to be due to small polar deviations from the parent symmetry [36].

The compound, $K_6Fe_{10}F_{30}$ (alternatively formulated as $K_{0.6}Fe^{2+}_{0.6}Fe^{3+}_{0.4}F_3$), crystallizes in TTB structure type, with a polar orthorhombic distortion (space group Pba2, $c = 2c_{TTB}$) at room temperature [37], deriving from the ideal TTB P4/mbm tetragonal phase. In the TTB-derived fluoride, "KFe_2F_6", two structural phase transitions occur between nonpolar phases P4/mbm ↔ Pbam ↔ G2 at $T_1 = 340$ K and $T_2 = 250$ K without any doubling of unit cell parameters, followed by a magnetic phase transition at lower temperature ($T_N = 133$ K) [38]. In the P4/mbm form, Fe^{2+} and Fe^{3+} ions are not ordered and distributed between Fe1 and Fe2 sites, whereas in the Pbam one Fe2 site is split into two sites, Fe2 and Fe3, as shown in Fig. 8.

7. Heat capacity and magnetic properties of $CsFe_2F_6$ exhibiting the defect-pyrochlore structure

For x close to 0.5 and large monovalent cations, mixed-valency iron fluorides, A_xMF_3 (A= Rb, Cs, Tl, NH_4) display a structural arrangement of the defect-pyrochlore type (see Table 1). For $CsFe^{2+}Fe^{3+}F_6$, the ordered arrangement of $Fe^{2+}$and Fe^{3+} ions in the two cationic sites of the pyrochlore structure have been confirmed by Mössbauer spectroscopy. Pyrochlore-type $CsFe_2F_6$ indeed contains two nonequivalent octahedral

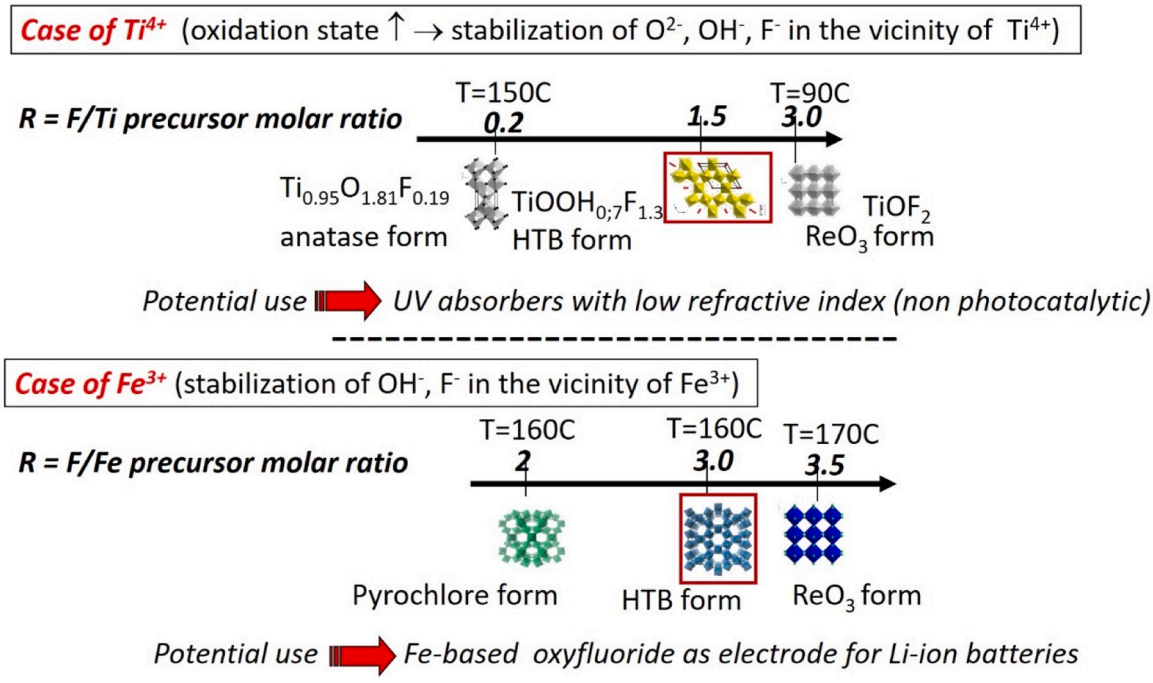

Fig. 6. Dependence of the type of final Ti^{4+} and Fe^{3+} (oxy)hydroxyfluorides on the experimental parameters (R ratio) used in the microwave-assisted synthetic route (from ref. 30).

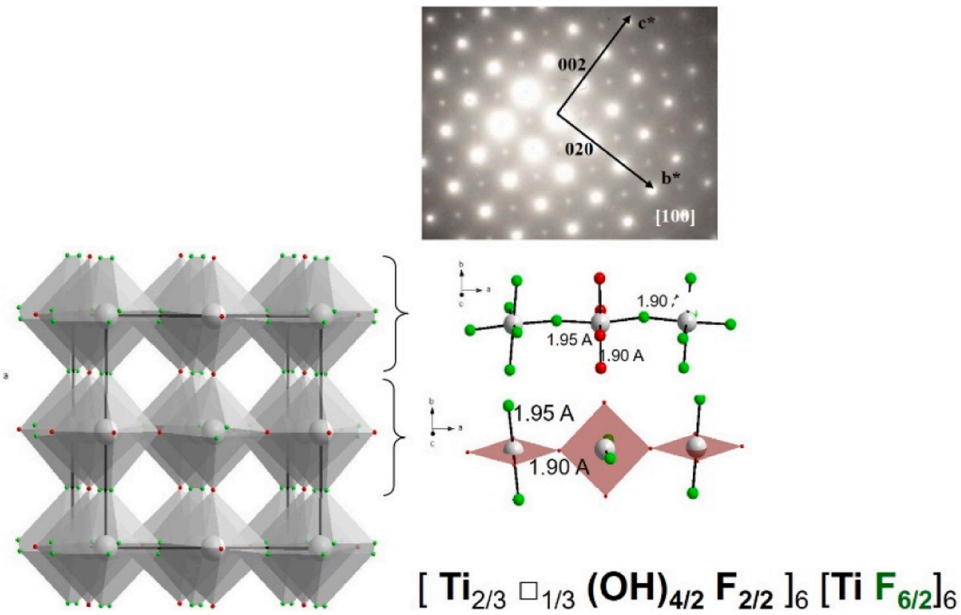

Fig. 7. Structural network and TEM photograph of the supercell (SG: Pn$\bar{3}$m, a = 7.6177 Å) of $Ti_{0.75}\square_{0.25}(OH)_{1.5}F_{1.5}$. The two Ti sites and the two O/F atomic positions characterizing Ti^{4+} cations and O^{2-}/F^{-} anions ordering pointing outwards [from ref. 28].

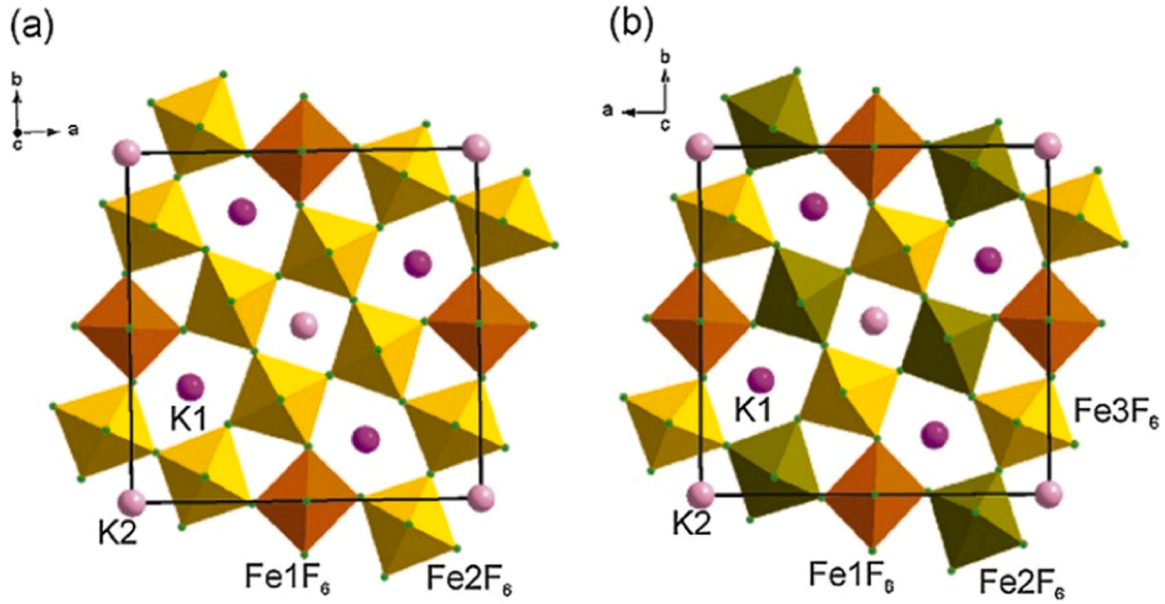

Fig. 8. Crystal structure of KFe_2F_6 at: (a) T = 453 K, P4/mbm; (b) T = 303 K, Pbam [from ref. 38].

sites for iron cations. The Fe1 site is located in an elongated FeF_6 octahedron, whereas Fe2 position is in a slightly compressed one. The octahedral environments of the Fe1 and Fe2 cationic sites are given in Fig. 9, together with the qualitative energy levels in an octahedral crystal field for 3d orbitals. Due to their high-spin electronic configurations and a larger available volume, Fe^{2+} cations are more suitable for the Fe2 positions. Mössbauer experiments confirm the ordered distribution of Fe^{3+} and Fe^{2+} in Fe1and Fe2 positions, respectively.

In a narrow temperature range, i.e., 500–560 K, a succession of phase transitions occur as determined by differential scanning calorimetry (DSC) in $CsFe^{II}Fe^{III}F_6$: Pnma (Z=4) ↔ Imma (Z = 4) ↔ $I4_1/amd$ (Z = 4) ↔ Fd$\bar{3}$m (Z = 8) (from lower to higher-temperature). The rotation of (FeF_6) octahedra and small displacements of Fe atoms are responsible of the structural phase transitions. The low experimental entropy values that are associated with these transitions are characteristic of displacive transformations [40]. The structure of the high temperature (Fd$\bar{3}$m) form and the low-temperature (Pnma) form are compared in Fig. 10**.** In the structure of the cubic form at 573 K, the cluster of five (FeF_6) octahedra is not tilted, whereas in the orthorhombic Pnma form at 298 K the (FeF_6) clusters rotate around the b_{orth}-axis but not along a_{orth}-axis [39]. The determination of the magnetic structure of the low-temperature form of $CsFe_2F_6$ requires the existence of four sublattices. Sublattices 1 and 2 contain Fe^{3+} cations and sublattices 3 and 4 are occupied by Fe^{2+} cations . The relative orientations of the magnetic moments of Fe ions are shown in Fig. 11. A simple model of superexchange rules [3,41] can be used to estimate exchange interactions and magnetic structures. Exchange interactions in $CsFe_2F_6$, E_e (in K), are calculated using $E_e = z_{ij}J_{ij}S_iS_j$. The strongest interactions are antiparallel between Fe1 and Fe2 sites and to a lower level between Fe3 and Fe4, whereas frustrated interactions occur between Fe1-Fe3 and Fe2-Fe4.

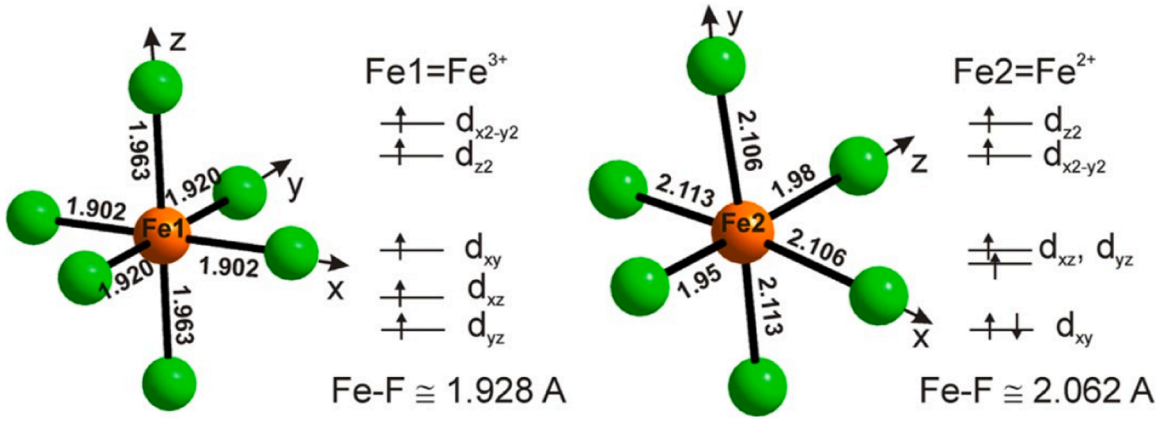

Fig. 9. Bond lengths in the two crystallographic sites of $CsFe_2F_6$, and the electronic splitting of the 3d-levels of Fe^{2+} and Fe^{3+}cations [from ref. 39].

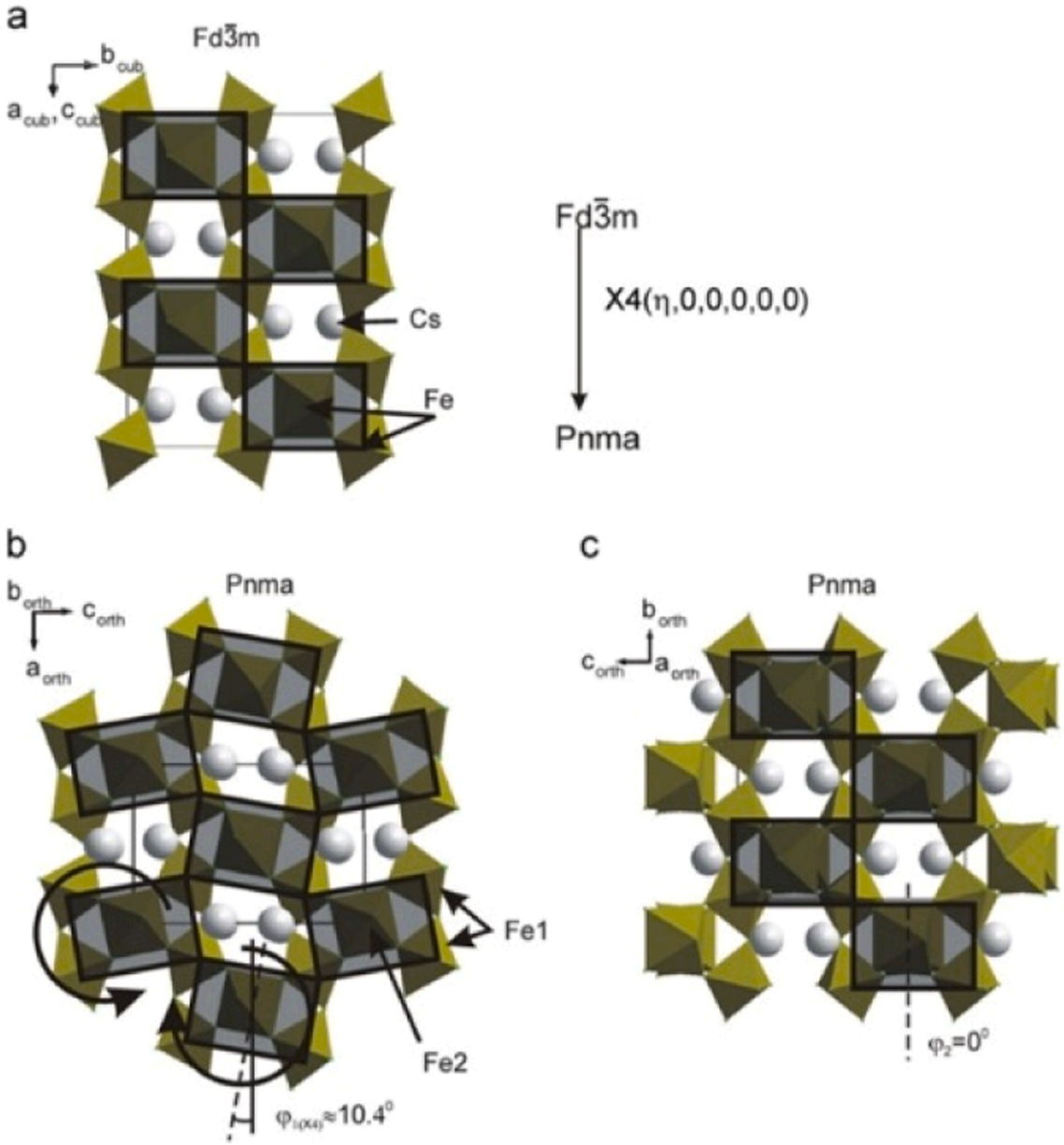

Fig. 10. a) Cubic form of $CsFe_2F_6$ at 573 K, illustrating clusters composed of five FeF_6 octahedra); b, c) orthorhombic form at 298 K (with FeF_6 clusters rotating around b_{orth}-axis and not along a_{orth}-axis) [from ref. 40].

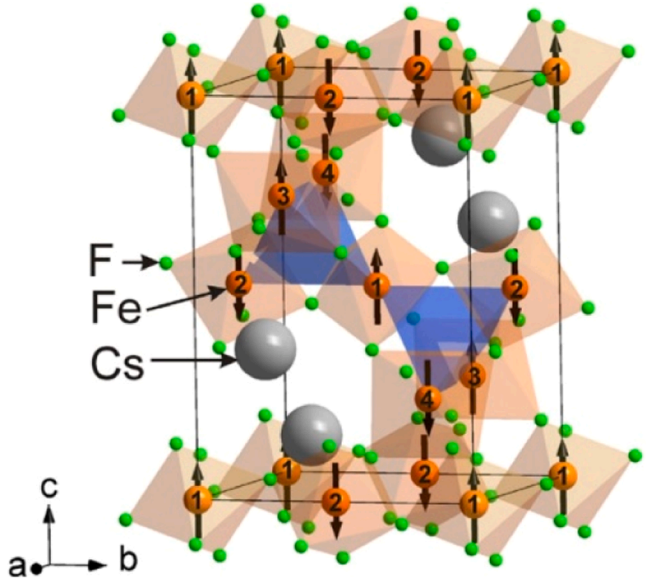

Fig. 11. Magnetic structure of $CsFe_2F_6$ shown with relative orientations of the magnetic moments of Fe ions [from ref. 39].

The magnetic data are: $T_N = 34$ K and a paramagnetic Curie temperature $\Theta_C = -260$K, and the major information arising from the very high value of the ratio (Θ_C/T_N) indicates the existence of strong frustration effects between layers in the structure. At 13.7 K and 30 K, heat capacity anomalies can be correlated with the structural phase transition. An antiferromagnetic ordering is observed associated with a Schottky anomaly. The orthorhombic symmetry is maintained down to 7 K, as revealed by the Raman spectra. The maximum magnetic entropy, as calculated for high-spin state $Fe^{2+}$and Fe^{3+} ions, is in good agreement with the total experimental magnetic entropy. It can be pointed out that a similar pyrochlore-type compound $CsMn^{2+}Mn^{3+}F_6$ was obtained using Cl^- anions under hydrothermal conditions for the mild reduction of Mn_2O_3 in concentrated HF. A magnetic transition to a canted antiferromagnet state was observed at 24.1 K, with successive long-range ordering of the Mn^{2+} and Mn^{3+} sites [42].

Note added in the proof: Mixed-metal fluorides with the HTB-type: $A_xM_x^{2+}M_{(1-x)}^{3+}F_3$, where x = 0.18−0.33 (A = Cs, Rb; M^{2+} = Co^{2+}, Ni^{2+}, Zn^{2+}; M^{3+} = V^{3+}) were recently synthesized using a mild hydrothermal method. Most of these phases crystallize in the monoclinic space group $P2_1/m$, except $Cs_{0.27}Zn_{0.27}V_{0.73}F_3$ which exhibits the $P2_1$ space group. These phases exhibit a HTB to cubic β-pyrochlore structural phase transition at high temperatures [43].

8. Conclusions

The variety of results obtained over the past 60 years for fluorides having the formula A_xMF_3 which exhibit structures derived from ReO_3, perovskite, defect-pyrochlore, hexagonal- and tetragonal- tungsten bronze types show the relevance of these materials to energy storage, catalysis, optical properties (luminescence, up- and down-conversion, UV absorption), magnetism, ferroelasticity and other fields. It is noteworthy that the ease of obtaining these fluoro-compounds in the form of nanoparticles has also opened up great possibilities in fields as varied as the material sciences, pharmaceuticals, medicine, and agrochemicals [44].

CRediT authorship contribution statement

Alain Tressaud: Supervision, Methodology, Investigation, Conceptualization.

Declaration of competing interest

There are no conflict to declare.

Acknowledgments

The author dedicates this review to the memory of Paul Hagenmuller (1921–2017) and Neil Bartlett (1936–2008), pioneers in solid state chemistry and in fluorine chemistry. ICMCB's colleagues Alain Demourgues, Etienne Durand, Damien Dambournet, Nicolas Penin, and my great friend Jean Grannec (1940–2023), members of the ICMCB Fluorine Group, are deeply acknowledged for their strong and fruitful contributions in these studies. Many thanks also to Henri Groult (Sorbonne Univ., Paris) for electrochemical investigations, Marc Leblanc and Vincent Maisonneuve (Univ. Le Mans, France) for sharing their extensive knowledge of fluoride structural networks, and my "old" colleague and friend Jacques Darriet for outstanding structure determinations. Concerning the different topics presented in this review, scientific cooperations have been established with scientists worldwide, such as Igor N. Flerov and Kirill S. Aleksandrov (1931-2010) (Kirensky Institute of Physics, Krasnoyarsk, Russia), Larisa Demyanova (Russian Academy of Sciences, Blagoveshchensk, Russia), Pavel Fedorov, (Russian Academy of Sciences, General Physics Institute, Moscow, Russia), Erhard Kemnitz and Michael Feist (Humboldt University, Berlin, Germany), Dietrich Babel and Werner Massa (Philipps Univ., Marburg, Germany), Boris Žemva (1940–2023) and Karel (Drago) Lutar (1947–2000) (Jožef Stefan Institute, Ljubljana, Slovenia), Tsuyoshi Nakajima (Aichi Institute of Technology, Japan), Hidekazu Touhara (Shinshu Univ., Japan).

Data availability

Data will be made available on request.

References

[1] L. Pauling, The Nature of the Chemical Bond and the Structure of Molecules and Crystals, Cornell Univ. Press, 1939.
[2] T. Nguyen, R.J. Cava, Hexagonal perovskites as quantum materials, Chem. Rev. 121 (2021) 2935–2965.
[3] J.B. Goodenough, Magnetism and the Chemical Bond, Interscience Publication, 1963.
[4] R. de Pape, Une série de composés fluorés de type bronze, C. R. Acad. Sci. 260 (1965) 4527–4530.
[5] A. Magnéli, Tungsten bronzes containing six-membered rings of WO_6 octahedra, Nature 169 (1952) 791–792.
[6] A. Tressaud, R. De Pape, J. Portier, P. Hagenmuller, Les systèmes MF-FeF_2 (M = Li, Na, Rb, Tl), C.R. Acad. Sc. 266 (1968) 984–986.
[7] J. Portier, A. Tressaud, R. De Pape, P. Hagenmuller, Classification structurale de divers composés fluorés du fer et de cations monovalents. Applications à leurs propriétés magnétiques, Mat. Res. Bull. 3 (1968) 433–436.
[8] R. De Pape, A. Tressaud, J. Portier, Sur de nouvelles séries de bronzes fluorés de composition MxFeF3 (M = Na, Rb, Tl), Mat. Res. Bull. 3 (1968) 753–758.
[9] A. Tressaud, Structural and Magnetic Correlations in Iron Fluorides, Ph. D. thesis, in: Structural and Magnetic Correlations in Iron Fluorides, 1, Univ. Bordeaux, 1969.
[10] A. Tressaud, R. De Pape, J. Portier, Les pyrochlores lacunaires MxFeF3 (M = R, Cs, Tl, NH4), C.R. Acad. Sc. 270 (1970) 726–728.
[11] A. Tressaud, R. De Pape, J. Portier, P. Hagenmuller, Les bronzes fluorés MxFeF3 (M = Na, K, Rb, Cs, Tl, NH4), Bull. Soc. Chim. Fr 10 (1970) 3411–3413.
[12] M. Leblanc, J. Pannetier, G. Férey, R. de Pape, Single crystal refinement of the structure of rhombohedral FeF_3, Rev. Chim. Miner 22 (1985) 107–114.
[13] R. de Pape, G. Férey, A new form of FeF_3 with the pyrochlore structure: soft chemistry synthesis, crystal structure, thermal transitions and structural correlations with the other forms of FeF_3, Mater. Res. Bull. 21 (1986) 971–978.
[14] M. Leblanc, G. Férey, P. Chevalier, Y. Calage, R. de Pape, Hexagonal tungsten bronze-type Fe^{III} fluoride: $(H_2O)_{0.33}FeF_3$; crystal structure, magnetic properties, dehydration to a new form of iron trifluoride, J. Solid State Chem. 47 (1983) 53–58.
[15] D. Dambournet, A. Demourgues, C. Martineau, S. Pechev, J. Lhoste, J. Majimel, A. Vimont, J.C. Lavalley, C. Legein, J.Y. Buzaré, F. Fayon, A. Tressaud, Nanostructured aluminium hydroxyfluorides derived from β-AlF_3, Chem Mater. 20 (2008) 1459–1469.
[16] D. Dambournet, A. Demourgues, A. Tressaud, Microwave-assisted hydrothermal route towards F-nanomaterials, in: A. Tressaud (Ed.), Functionalized Inorganic Fluorides, John Wiley &Sons, 2010, pp. 39–68, chapter 2.

[17] D. Dambournet, G. Eltanamy, A. Vimont, J.C. Lavalley, J.M. Goupil, A. Demourgues, E. Durand, J. Majimel, S. Rüdiger, E. Kemnitz, J.M. Winfield, A. Tressaud, Coupling sol–gel synthesis and micro wave-assisted techniques: a new route from amorphous to crystalline high-surface-area aluminium fluoride, Chem. Eur. J. 14 (2008) 6205–6212.
[18] E. Kemnitz, D. Menz, Fluorinated metal oxides and metal fluorides as heterogeneous catalysts, Prog. Solid State Chem. 26 (1998) 97–153.
[19] E. Kemnitz, G. Scholz, S. Rüdiger, Sol-gel synthesis of nanoscaled metal fluorides: mechanism and properties, in: A. Tressaud (Ed.), Functionalized Inorganic Fluorides, John Wiley &Sons, 2010, pp. 1–38, chapter 1.
[20] S. Rüdiger, G. Eltanany, U. Gross, E. Kemnitz, Real sol-gel synthesis of catalytically active aluminium fluoride, J. Sol-Gel Sci. Technol. 41 (2007) 299–311.
[21] A.Le Bail, C. Jacoboni, M. Leblanc, R. de Pape, H. Duroy, J.L. Fourquet, Crystal structure of the metastable form of aluminum trifluoride β-AlF_3 and the gallium and indium homologs, J. Solid State Chem. 77 (1988) 96–101.
[22] E. Kemnitz, U. Gross, St. Rüdiger, G. Scholz, D. Heidemann, S.I. Troyanov, I. V. Morosov, M.-H. Lemee-Cailleau, Comparative structural investigation of aluminium fluoride solvates, Solid State Sci 8 (2006) 1443–1452.
[23] D. Dambournet, Sur de Nouveaux Composés Hydroxyfluores Nanostructures à Base D'aluminium: Synthèses, Structures & Propriétés Acides (Lewis/Bronsted), Ph.D. Thesis, University Bordeaux1, January 2008.
[24] A. Tressaud, Structural architecture and physical properties of some inorganic fluoride series, J. Fluor. Chem. 132 (2011) 651–659.
[25] M. Duttine, D. Dambournet, N. Penin, D. Carlier, A.Wattiaux L.Bourgeois, K. W. Chapman, P.J. Chupas, H. Groult, E. Durand, A. Demourgues, Tailoring the composition of a mixed anion iron-based fluoride compound: evidence for anionic vacancy and electrochemical performance in Li cells, Chem. Mater. 26 (2014) 4190–4199.
[26] K. Lemoine, A. Hémon-Ribaud, M. Leblanc, J. Lhoste, J.M. Tarascon, V. Maisonneuve, Fluorinated materials as positive electrodes for Li- and Na-ion batteries, Chem. Rev. 122 (2022) 14405–14439.
[27] J. Meng, Z. Xiao, L. Zhu, X. Zhang, X. Hong, Y. Jia, F. Liu, Q. Pang, Fluorinated electrode materials for high-energy batteries, Matter 6 (2023) 1685–1716.
[28] A. Demourgues, N. Penin, E. Durand, E.F. Weill, D. Dambournet, N. Viadere, A. Tressaud, New titanium hydroxyfluoride $Ti_{0.75}(OH)_{1.5}F_{1.5}$ as a UV absorber, Chem. Mater 21 (2009) 1275–1283.
[29] X. Rocquefelte, F. Goubin, Y. Montardi, N. Viadere, A. Demourgues, A. Tressaud, M.H. Whangbo, S. Jobic, Analysis of the refractive index of TiO_2, $TiOF_2$, and TiF_4: concept of optical channel as a guide for understanding and designing optical materials, Inorg. Chem. 44 (2005) 3589–3593.
[30] A. Demourgues, L. Sronek, N. Penin, New nanostructured fluorocompounds as UV-absorbers (Ed.), in: A. Tressaud (Ed.), Functionalized Inorganic Fluorides, John Wiley &Sons, 2010, pp. 229–271. chapter 8.
[31] N. Penin, N. Viadere, D. Dambournet, A. Tressaud, A. Demourgues, Evolution of the optical band gap in titanium-based oxy(hydroxy) fluorides series, Mater. Res. Soc. Symp. Proc. (2006) 891.
[32] P. Poizot, S. Laruelle, S. Grugeon, L. Dupont, J.M. Tarascon, Nano-sized transition-metal oxides as negative-electrode materials for lithium-ion batteries, Nature 407 (2000) 496–499.
[33] N. Pereira, F. Badway, M. Wartelsky, S. Gunn, G.G. Amatucci, Iron oxyfluorides as high capacity cathode materials for lithium batteries, J. Electrochem. Soc. 156 (2009) A407.
[34] M. Bervas, L.C. Klein, G.G. Amatucci, Reversible conversion reactions with lithium in bismuth oxyfluoride nanocomposites, J. Electrochem. Soc. 153 (2006) A159–A170.
[35] D. Dambournet, K.W. Chapman, P.J. Chupas, R.E. Gerald II, C.Labrugere N.Penin, A. Demourgues, A. Tressaud, I. Belharouak, K. Amine, Mixed lithium insertion and conversion mechanism in a titanium-based mixed anion nanocomposite, J. Amer. Chem. Soc. 133 (2011) 13240–13243.
[36] J. Ravez, S. Abraham, R. de Pape, Ferroelectric-ferroelastic properties of $K_3Fe_5F_{15}$ and the phase transition at 490 K, J. Appl. Phys. 65 (1989) 3987–3990.
[37] D. Pajić, Z. Jagličić, Z. Trontelj, Slow magnetic dynamics in the $K_3M^{II}_3M^{III}_2F_{15}$ multiferroic system, J. Appl. Phys. 112 (2012) 073908.
[38] M.V. Gorev, I.N. Flerov, A. Tressaud, M.S. Molokeev, A.V. Kartashev, E. I. Pogoreltsev, O.A. Bayukov, Phase transitions in fluoride KFe_2F_6 with tetragonal tungsten bronze structure, J. Fluor. Chem. 168 (2014) 204–211.
[39] M.V. Gorev, I.N. Flerov, A. Tressaud, E.V. Bogdanov, A.V. Kartashev, O. A. Bayukov, E.V. Eremin, A.S. Krylov, Heat capacity and magnetic properties of fluoride $CsFe^{2+}Fe^{3+}F_6$ with defect pyrochlore structure, J. Solid State Chem. 237 (2016) 330–335.
[40] M.S. Molokeev, E.V. Bogdanov, S.V. Misyul, A. Tressaud, I.N. Flerov, Crystal structure and phase transition mechanisms in $CsFe_2F_6$, J. Solid State Chem. 200 (2013) 157–164.
[41] P.W. Anderson, New approach to the theory of superexchange interactions, Phys. Rev. 115 (1958) 2–13.
[42] V.V. Klepov, K.A. Pace, A.A. Berseneva, J.B. Felder, S. Calder, G. Morrison, Q. Zhang, M.J. Kirkham, D.S. Parker, H.C. Zur Loye, Chloride reduction of Mn^{3+} in mild hydrothermal synthesis of a charge ordered defect pyrochlore, $CsMn^{2+}Mn^{3+}F_6$, a canted antiferromagnet with a hard ferromagnetic component, J. Am. Chem. Soc. 143 (2021) 11554–11567.
[43] L.W. Masachchi, N. Keerthisinghe, A.A. Berseneva, G. Morrison, M.D. Smith, L. S. Breton, J. Schorne-Pinto, M. Aziziha, H.C. zur Loye, Sensitivity of mild hydrothermal synthesis to the reaction conditions: targeting mixed-metal hexagonal tungsten bronze fluorides $A_xM^{2+}_xM^{3+}_{(1-x)}F_3$ to investigate their magnetic behavior, Inorg. Chem. 63 (2024) 17598–17607.
[44] A. Tressaud (Ed.), "Progress in fluorine science" series, Elsevier, Amsterdam; 2016-2019: Vol. 1- A. Tressaud, K. Poeppelmeier (Eds.), Photonic & electronic properties of fluoride materials, 2016 //Vol.2- O. Boltalina, T. Nakajima, (Eds.), New forms of fluorinated carbons, 2016 // Vol. 3- H. Groult, F. Leroux, A. Tressaud (Eds), Modern synthesis processes and reactivity of fluorinated compounds, 2017 // Vol. 4- G. Haufe, F.Leroux (Eds.), Fluorine & Health: Pharmaceuticals, Medicinal Diagnostics, and Agrochemicals, 2018. // Vol. 5- A. Tressaud, Fluorine, a Paradoxical Element, 2019.